Comparison of measured current density distributions at PEFC with calculated distributions by using measured membrane properties

Kazuo ONDA, Hironori KOORI, Takuya TANIUCHI and Takuto ARAKI

Department of Electrical and Electronics Engineering
Toyohashi University of Technology, Toyohashi 441-8580
JAPAN
E-mail: onda@eee.tut.ac.jp

Abstract

The water management factors such as transmissivity and electro-osmotic coefficient of water vapor through the membrane and power loss factors such as activative and resistive overpotentials were measured. The numerical distributions of current density under various operating conditions agreed well with the measured distributions by segmented electrodes.

Keywords: Polymer Electrolyte Fuel Cell, Current density distribution, Membrane properties measurement

1. Introduction

Since membrane physical properties have significant impacts on the performance of Polymer Electrolyte Fuel Cell(PEFC), it is necessary to know the water management factors such as transmissivity and electro-osmotic coefficient of water vapor through the membrane-electrode assembly (MEA), and power loss factors such as activation and resistive overpotentials. Nevertheless, the effects by these factors on PEFC are not cleared sufficiently. The objective of the present investigation is set to obtain basic information of the membrane properties and to establish a numerical code, which can describe well the performance of PEFC.

2. Measurements of Membrane Properties and Overpotentials

2.1 Experimental Apparatus

An overview of the experimental apparatus is illustrated in Fig.1. Air and modified reformed

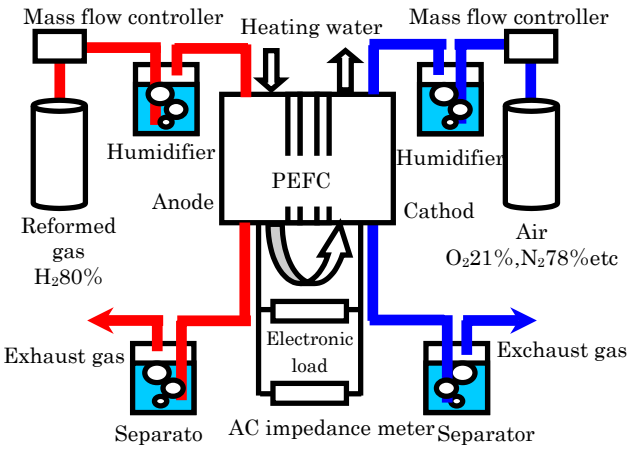

Figure1. Experimental apparatus

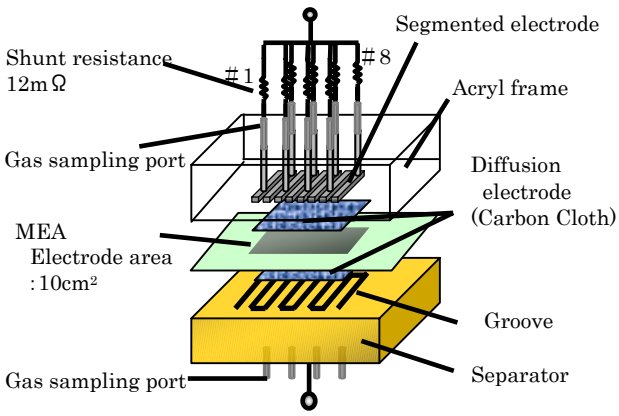

Figure 2. Configuration of cell and segmented electrodes

fuel from gas cylinders are regulated by mass flow controllers, and led to fuel cell(FC). The humidifiers placed before FC control the dew-point temperatures of air and fuel. Electronic resistive load (PLZ-152WA, Kikusui Elec. Co.) is connected to FC instead of actual loading, and measuring the current and voltage of FC. Figure 2 shows the FC assembly, where the MEA (Gore Select, Japan Gore-Tex Inc.) of 20μm thickness is set between the two electrodes. Carbon cloths are inserted between the MEA and separators as diffusion electrodes. One side of which consist of segmented electrodes with grooves for air or fuel supply and the segmented electrodes are mold in an electrically insulating plate as shown in Figure 2, for measuring current density distributions. Additionally, several holes are drilled in the grooves to measure concentration changes of hydrogen and oxigen to get another current density distribution.

2.2 Water Vapor Diffusivity through Diffusion Electrodes, and Transmissivity and Electro-osmotic coefficient through MEA

To obtain the diffusive properties, the cell outlet humidities at both anode and cathode were measured with supplying different humidities to both FC inlets. The measurement procedure was essentially the same as those described previously(1). Measured water vapor diffusivity for diffusion electrode D_{diff} at cell temperature T_{mem}=50˚C and 60˚C are plotted in Fig. 3. The diffusivity did not change against relative humidity. This result is consistent with a simple following equation,

$$D_{diff} = f \cdot D_{Air-H_2O} \tag{1}$$

where $D_{Air\text{-}H2O}$ is water vapor diffusivity in air, and f is effective porosity of diffusion electrodes. In the case of out carbon cloth, f is calculated to be about 0.25.
Transmissivity through MEA Tr is also shown in Fig. 3. Our measured Tr was about 7 times higher than the ones by Nguyen *et. al.*(2) and lower than ones by Yamada *et.al.*(3). However, the tendency of Tr, which rose as relative humidity increase, was consistent with those by Nguyen *et.al*. So we approximate Tr as to 7 times greater than those of Nguyen *et.al*.
Electro-osmotic coefficients n_d are determined similarly with the diffusion coefficient except that the electric current was made flow to transport water electro-osmotically. Figure 4 shows the n_d as a function of relative humidity. The electro-osmotic coefficient n_d became large when the humidity increases. n_d at MEA temperature of 50˚C agreed with that by Nguyen *et.al.*(2). n_d by Yamada who performed similar experiment with us was almost same as ours especially in a case of using carbon cloth, however, the tendency of n_d against humidity was inverse.

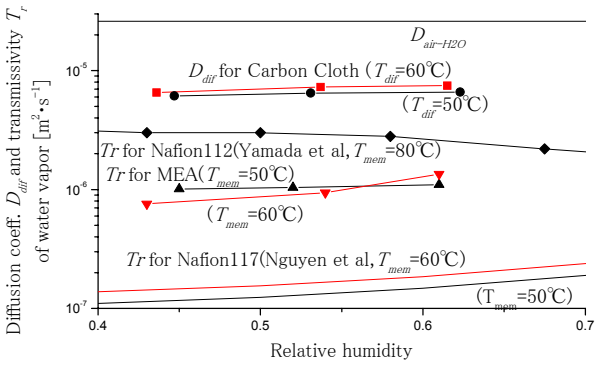

Figure 3. Change of Tr and D_{diff} of water vapor by relative humidity

2.3 Ionic Resistivity and Activation Overpotential of MEA

Resistive and activative overpotentials are important factors of PEFC power generation performance. The ionic resistance was measured by AC impedance meter (SOLARTRON SI1280B), supplying air with the same humidity to both anode and cathode to avoid the movement of water through MEA. The parameters for MEA resistance are the membrane temperature T_{mem} and the flow relative humidity a. The measured MEA resistivity is plotted against relative humidity a in Fig. 5. The resistivity did not depend on the membrane temperature, but depended only on relative humidity a. Therefore the following experimental ionic resistivity ρ, a function of only relative humidity a, was employed in the following numerical analysis.

$$\rho = 57.3 + 383.\exp\left(-\frac{a-0.089}{0.049}\right) + 244\exp\left(-\frac{a-0.089}{0.268}\right) \qquad [\Omega\cdot\mathrm{cm}] \qquad (2)$$

For measuring activation overpotential η_{act}, the relatively high flow rates of 600cc/min were provided to hold the low utilization rate of H_2 and O_2 in order to prevent variation of η_{act} along the flow by the distributed current density. η_{act} was derived by subtracting the cell voltage V_{cell} and the resistive overpotential ir from the Nernst potential V_{Nernst} as follows.

$$\eta_{act} = V_{Nernst} - V_{cell} - ir \qquad [\mathrm{V}] \qquad (3)$$

Here, the spatially averaged partial pressures of active materials were used to determine V_{Nernst} considering water vapor pressures. The experimental conditions for η_{act} measurement were as follows; FC temperature : 60˚C, cathode O_2 partial pressure P_{O_2} : 0.05, 0.2, 1.0; anode H_2 partial pressure P_{H_2} : 1.0. Figure 6 shows the change of activation overpotential by oxygen concentration and current density. The activation overpotential increased almost linearly except for the region of very low current density where is not so important for practical application. Therefore we employed the following empirical formula in the following numerical analysis.

$$\eta_{act} = \frac{0.065}{P_{O_2}^{0.81}} i + 0.455 \qquad [\mathrm{V}] \qquad (4)$$

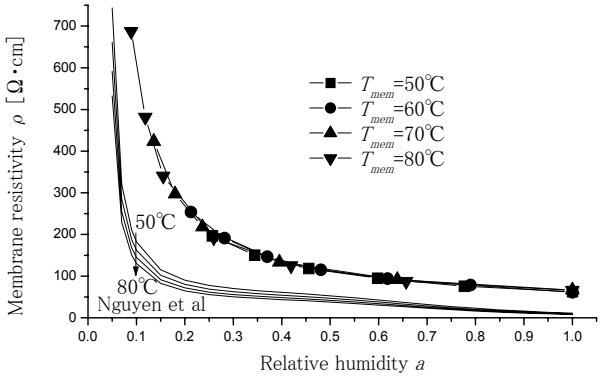

Figure 5. Change of membrane resistance by relative humidity

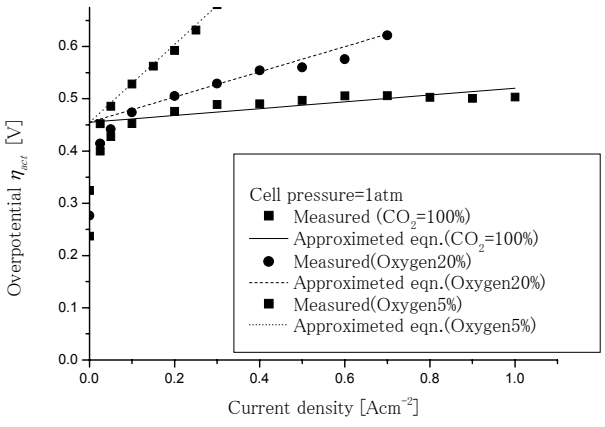

Figure 6 Change of membrane resistance by relative humidity

2.4 Measurement of Current Distribution

Current distributions were measured by two different methods to confirm the reliability of measurement. First method adopted the segmented electrodes cell to measure the current distribution by shunt resistances. Another method adopted gas chromatography to measure gas composition changes to be converted to the current distribution through the decreased flow rate of H_2 or O_2. N_2 mixture fuel and air were employed in this measurement to keep the constant flow rate of N_2 as reference. H_2 gas mixed with 20% N_2 (not CO_2) was used as fuel, because CO_2 is easy to be solved in water and not giving the correct reference.
Figure 7 and 8 show the measured current densities for two average current density of 0.3A/cm^2 and 0.4A/cm^2, respectively. The current density estimated by gas chromatography fluctuated to some extent, but are compatible with that by the segmented electrodes cell. Thus we could confirm the measurement reliability of current density distribution by two methods.

3. Numerical Analysis of Power Generating Performance

3.1 Computational Procedure

Following assumptions were adapted to our numerical analysis[4].

1. Parallel flow type fuel cell is targeted.
2. There are 8 parallel grooves for each side of fuel and air separator, and all of the grooves have the same flow rate and performance.
3. The gas flow along the groove is assumed to be plug flow.
4. Owing to the constant temperature water, which is circulated through separator, the cell temperature is assumed to be kept constant.
5. Effect of flooding due to generated water at cathode is ignored.

Control volume method was used to solve the simultaneous equations for mass and charge, energy conservation equations with an equivalent electric circuit for FC. The energy conservation equation for MEA is shown in appendix as a representative equations for equation for every conservation. The Nernst potential is given by

$$V_{Nernst} = E^0 + \frac{RT_{mem}}{2F} \ln \frac{P_{H_2} P_{O_2}^{0.5}}{P_{H_2O,c}} \tag{8}$$

The resistance overpotential is given by the following integration of membrane resistivity through its thickness t_{mem}.

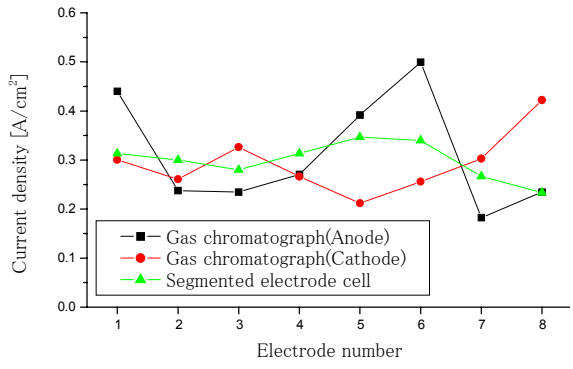

Figure 7. Comparison of measured current distributions i mean I=0.3A/cm^2

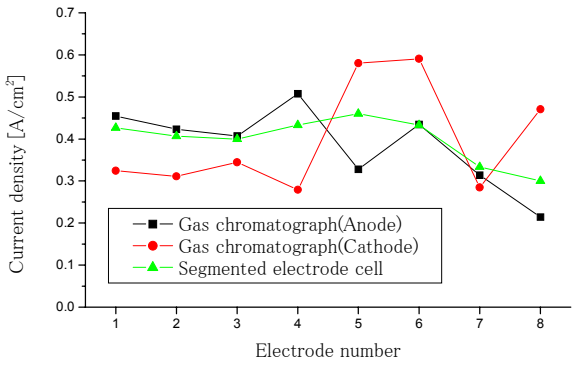

Figure 8. Comparison of measured current distributions i mean I=0.4A/cm^2

$$\eta_{ohm} = \left(\frac{1}{a_a - a_c} \int_{a_c}^{a_a} \rho da \right) t_{mem} i \qquad (9)$$

3.2 Results of Current Distribution Numerical Analysis

The current density distributions calculated by the numerical simulation are shown in Fig. 9, 10 and 11. The conditions used in the analysis are summarized in Table 1. The agreement between the numerical and measured results was good on the whole. The measured showed higher current density at inlet, and lower current density at outlet than the calculated. This discrepancy might be due to the effect of generated water at a downstream cathode, hindering the site for electrochemical reaction. Especially in a situation with higher oxygen utilization ratio of 80%. The current density tends to increase at inlet when the current density decreases near outlet probably by the flooding. Revised empirical formula for the activation overpotential may lead the calculated results closer to the measured, but we are now trying to include the generated water in our simulation to avoid the performance degradation by water flooding.

Table 1 Experimental conditions used in analysis

	Fig.9	Fig.10	Fig.11
Cell temperature[℃]	60		
Anode flow rate[cc/min]	48		
Cathode flow rate[cc/min]	91	136	182
Anode dew temperature[℃]	60		
Cathode dew temperatuer[℃]	Not humidified		
Fuel and oxygen utilization ratio(i_m=0.2)	0.4-0.4	0.4-0.26	0.4-0.2
Fuel and oxygen utilization ratio(i_m=0.3)	0.6-0.6	0.6-0.4	0.6-0.3
Fuel and oxygen utilization ratio(i_m=0.4)	0.6-0.6	0.8-0.53	0.8-0.4

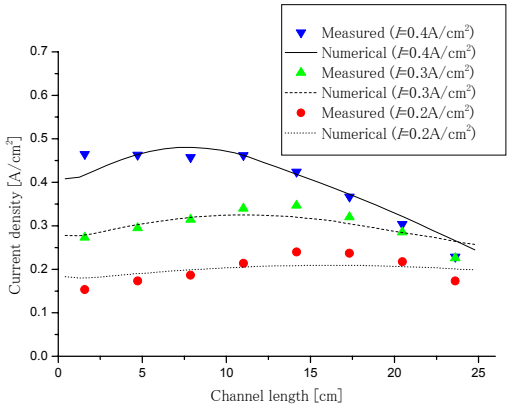

Figure 9 Comparison between the measured and the numerical (Air flow 90cc/min)

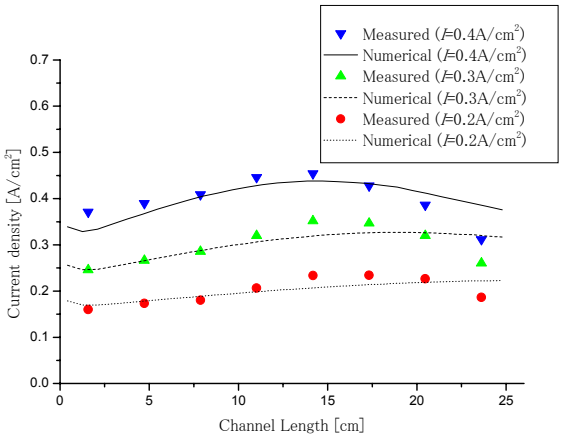

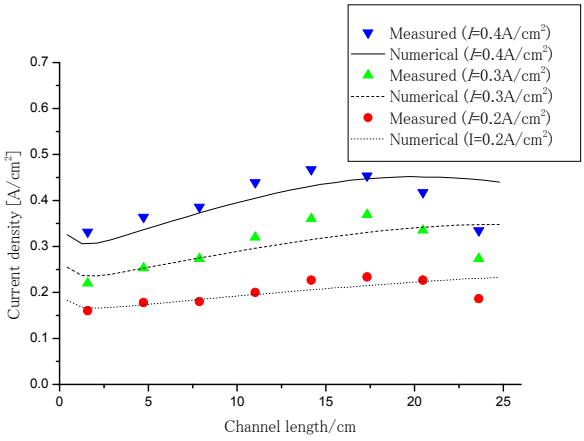

Figure 10. Comparison between the measured and the numerical (Air flow rate of 135cc/min)

4. Conclusion

The water management factors such as transmissivity and electro-osmotic coefficient of water vapor through the membrane electrode assembly, and power loss factors such as activative and resistive overpotentials have been measured. These factors were adopted to analyze our experimental results of PEFC power generation tests by our two-dimensional simulation code. The code considers simultaneously the mass, charge and energy conservation equations with the equivalent electric-circuit for PEFC to give numerical distribution of hydrogen/oxygen concentrations, current density, and gas/cell-component temperatures along gas flow. The calculated distributions of current density under various operating conditions have agreed well with the measured distributions at segmented-electrodes cell. Hydrogen /Oxygen concentration changes measured by gas chromatography along the gas flows have also given the experimental current distributions, which coincides almost with that by the segmented-electrodes. Degradation factors for cell performance were also discussed from the numerical results by the simulation code. Also further improvements for out experiment and analysis have been pointed out.

Appendix

Energy conservation equation for MEA as as represent ative one for other elements.

$$
\begin{aligned}
& t_{mem} w_{cell} \frac{d}{dy}\left(k_{mem} \frac{dT_{mem}}{dy} \right) \\
& = w_{cell} k_{dif,a-mem} \frac{T_{mem} - T_{dif,a}}{\Delta x_{diff,a-mem}} + w_{cell} k_{dif,c-mem} \frac{T_{mem} - T_{dif,c}}{\Delta x_{dif,c-mem}} \\
& \quad - w_{cell} \{ N_{H_2,a} H_{H_2 - T_{dif,a}} - N_{O_2,c} H_{O_2 - T_{dif,c}} \\
& \quad + N_{vap,a} H_{vap - T_{dif,a}} - N_{vap,c} H_{vap - T_{dif,c}} \\
& \quad + N_{liq,a} H_{liq - T_{dif,a}} - N_{liq,c} H_{liq - T_{dif,c}} \} \\
& \quad - w_{cell} \left\{ N_{H_2} \Delta H_{LHV} - i(y)(V_{Nernst} - \eta_{ohm} - \eta_{act}) \right\}
\end{aligned}
\tag{10}
$$

References

[1] T.Kyakuno, K.Hattori, K.Ito and K. Onda, Proc. 15th IEEJ Conf., 2003. (in Japanese)

[2] T.V.Nguyen and R.E.White: A Water and Heat Management Model for Proton-Exchange-Membrane Fuel Cells. J. Electrochem. Soc., Vol.140, No8, 1993.

[3] H.Yamada and Y.Morimoto, Electro-osmotic Drag and Diffusion Coefficient of Water in Polymer Electrolyte Membrane. Proc. 70th anniversary Jpn. Electrochem. Soc. 2003. (in Japanese)

[4] T. Aoki, N. Miyauchi, K. Ito, Y. Inui and K. Onda: Numerical Analysis of Polymer Electrolyte Fuel Cell Using Empirical Equations for Overpotentials. Trans. IEE Japan, Vol. 122-B, No. 12, 2002 (in Japanese)